Simulation of Helical Flows in Microchannels

Friedhelm Schönfeld and Steffen Hardt
Institut für Mikrotechnik Mainz GmbH (IMM), 55129 Mainz, Germany

DOI 10.1002/aic.10071
Published online in Wiley InterScience (www.interscience.wiley.com).

Helical flows are investigated in structured microchannels with regard to micromixing by means of computational fluid dynamics (CFD). In the case of bas-relief structured channels the numerical results are found to be in good agreement with experimental findings. The magnitude of the transverse flow is computed for various Reynolds numbers and for different geometries including channels with bas-relief structures on two opposite walls. Transverse flows in structured microchannels are compared to secondary flow patterns in curved square channels. The corresponding helical flows are analyzed for Dean numbers ranging from 1 to 900. Special attention is paid to the occurrence of additional *vortices close to the center of the outer channel wall. Based on the results a new type of micromixer is proposed that relies on the transition of the secondary flow pattern from* two *to four vortices.* © 2004 American Institute of Chemical Engineers *AIChE J,* 50: 771–778, 2004

Keywords: helical flow, microchannel, computational fluid dynamics, micromixing, bas-relief structure

Introduction

Micromixers have attracted considerable attention for various applications in the fields of μ-TAS and Lab-on-a-Chip systems as well as chemical process technology. In contrast to macroscopic devices, microfluidic systems are mostly based on laminar flow. When mixing is not supported by the complex spatiotemporal patterns of turbulent flow, achieving an acceptable mixing quality on a short time scale becomes much more difficult. To enable fast and efficient mixing of liquids and gases in microfluidic systems, various principles have been used (Ehrfeld et al., 2000), two of the most prominent of which are multilamination mixers (Ehrfeld et al., 1999) and split-and-recombine mixers (Schwesinger et al., 1996). Even concepts with external agitation of the flow by ultrasound (Yang et al., 2001) have been discussed. Many of the principles developed so far are based on comparatively complex designs. However, for future highly integrated microfluidic systems simple and efficient mixing units are needed. Recently, a new type of micromixer has been presented that relies on the induction of transverse flows by means of bas-relief structures on the channel floor (Johnson et al., 2001, 2002; Kim et al., 2002; Stroock et al., 2002a,b). In contrast to many other designs such mixers are compact and relatively easy to fabricate. Because of the helical flow patterns induced by the bas-relief structures not only efficient mixing can be achieved, but also heat transfer from the channel walls is enhanced and hydrodynamic dispersion of concentration tracers transported through a channel is reduced.

In Stroock et al. (2002a,b) the magnitude of the transverse flow was derived experimentally from optical micrographs and compared to analytical results. Although the analytical model is somewhat simplified the authors find a reasonable agreement between both approaches.

For a reliable layout and optimization of such kinds of mixers methods of computational fluid dynamics (CFD) are needed because the analytical description can be used only in certain limits. In this article we present CFD results for bas-relief structured channels of various geometries. The transverse flow is found to be in good agreement with the experimental results presented in Stroock et al. (2002a). Next we analyze the dependency of the relative transverse velocity, that is, the ratio of the transverse velocity component and the axial velocity component, on the Reynolds number Re. For the range of Reynolds numbers considered we find only a small change in the relative transverse velocity with varying Re. Furthermore

Correspondence concerning this article should be addressed to F. Schönfeld at schoenfeld@imm-mainz.de.

the helical flow in channels with structures on two opposite walls is analyzed and the relative transverse velocity is found to be considerably increased.

The second part of the article is motivated by the fact that similar helical flows can be induced using simpler geometries. We show that the secondary flow in curved channels, known by the term "Dean vortices," can be used in a similar way as the bas-relief structured channels. The mixing efficiency of the latter is based not only on simple helical flows but also on chaotic flow patterns of alternating helical flows, which are achieved be means of so-called staggered-herringbone structures (Stroock et al., 2002b) or additional flow barriers (Kim et al., 2002). A similar sequence of flow patterns can also be achieved in simple curved channels. It turns out that the secondary flow pattern depends on the flow velocity, the position in the channel as well as on its hydraulic diameter, and radius of curvature. Depending on these parameters two qualitatively different secondary flow patterns with one or two pairs of counterrotating vortices can be induced, such that by successive "switching" between different flow patterns a chaotic flow can be generated and mixing can be improved. Note, the proposed mixer relies on the occurrence of *additional* vortices under certain flow conditions, periodic alterations of which allow achieving chaotic mixing within a simple curved channel of planar geometry. The proposed design is substantially different from other mixers relying on secondary flow effects [such as the helical-coil reactor investigated by Sawyers et al. (1996)].

In this article we analyze the secondary flow patterns of curved square channels of different dimensions. In particular we investigate the occurrence of the two additional vortices for various Dean numbers. Finally we compare the relative transverse flow of bas-relief structured channels to that of curved square channels.

The article is organized as follows. After a short outline of the mathematical framework the helical flow of bas-relief structured channels is analyzed for various structure heights. Next, helical flows of channels with one structured wall are compared to corresponding flows in channels with two structured walls. In the second part of the article helical flow patterns of curved square channels are analyzed. A summary and conclusion constitutes the final section.

Mathematical Framework

The numerical results presented in this work are based on the solution of the incompressible Navier–Stokes equation

$$\frac{\partial v_i}{\partial t} + (v_j \nabla_j) v_i = -\frac{1}{\rho} \nabla_i p + \frac{\eta}{\rho} \nabla^2 v_i, \quad \nabla_i v_i = 0 \qquad (1)$$

and a convection–diffusion equation for a concentration field

$$\frac{\partial c}{\partial t} + (v_i \nabla_i) c = D \nabla^2 c \qquad (2)$$

by means of the finite-volume method. v_i represents the components of the fluid velocity; ρ and η are its density and viscosity, respectively; D is the binary diffusion constant; and p and c denote density and concentration, respectively.

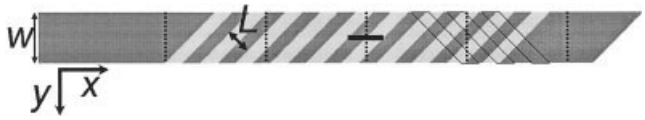

Figure 1. Geometry outline of the model used in the simulation of single-sided bas-relief structured channels.

Dark and light gray denote a channel height of $h(1 + \alpha)$ and $h(1 - \alpha)$, respectively, with $h = 0.079$ mm and α varying between 0.01 and 0.76. The channel width w equals 0.2 mm. The black patch in the center denotes the area that was used for integration of the velocity components.

Throughout the article the Einstein convention of summation over repeated indices is used. For pressure–velocity coupling, the SIMPLEC algorithm is used (Noll, 1993). For discretization of the species concentration Eq. 2 the QUICK differencing scheme is used. For velocities and pressure we used the "hybrid" and the "central" differencing scheme, respectively (CFX-4.2 Solver Manual, 1997). The simulations were performed with the commercial flow solvers CFX4 and CFX5 of AEA Technology.

Numerical errors, attributed to discretization of the convective term in Eq. 2, introduce an additional, nonphysical diffusion mechanism (see, for example, Fletcher, 1997). Especially for liquid mixing with characteristic diffusion constants in the order of 10^{-9} m^2/s, this so-called numerical diffusion (ND) is likely to dominate diffusive mass transfer on computational grids, given that typical Peclet numbers (vl/D) are of the order of 10 for typical cell dimensions (l) and velocities (v) used in the present study.

Because of ND artifacts, mixing was not simulated in detail. Instead, the corresponding convection–diffusion equation was solved with the diffusion coefficient D set to zero. The resulting concentration fields give an indication of how a solute is distributed in space. In this work we are mainly interested in the convective patterns redistributing the liquid transverse to the flow direction. By solving Eq. 2 the stretching, tilting, and thinning of liquid lamellae can be followed, and even if ND is superimposed onto the observed diffusive mass transfer, the computed concentration field gives important information on the characteristic dimensions of the lamellae and the mixing times to be expected.

Simulation of Helical Flow in Bas-Relief Structured Microchannels

The geometry of the simulated channel with a structured bottom wall is outlined in Figure 1. In the first simulation the dimensions corresponding to the bas-relief structured channel examined experimentally by Stroock et al. (2002a) were chosen: $w = 0.2$ mm, $h = 0.079$ mm, $L = 0.1$ mm, and $\alpha = 0.134$. The numerical model constitutes about 300,000 hexahedral elements with typical lateral dimension of 7 μm (width) and a typical height of 2.5 μm.

Because of the anisotropic flow resistance caused by the obliquely oriented ridges a twisted, helical flow is induced. At the top (bottom) of the channel, the transverse flow is in the y ($-y$)-direction (Johnson et al., 2001, 2002; Stroock et al., 2002a,b). To compare the magnitude of the transverse flow to the experimental results of Stroock et al. the velocity compo-

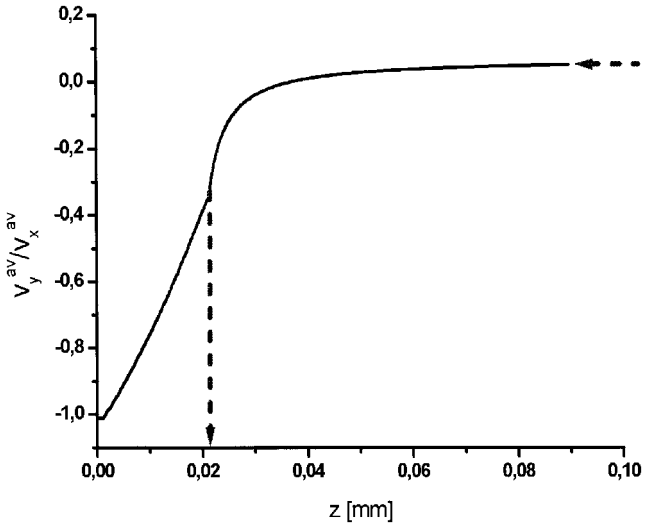

Figure 2. Averaged relative transverse velocity (i.e. ratio of the averaged velocity components) for h = 0.079 mm and α = 0.134.

The vertical arrow marks the edge of the bas-relief structures at a height of $2\alpha h$. The horizontal arrow marks the boundary value at the upper wall and is read off to be 0.052.

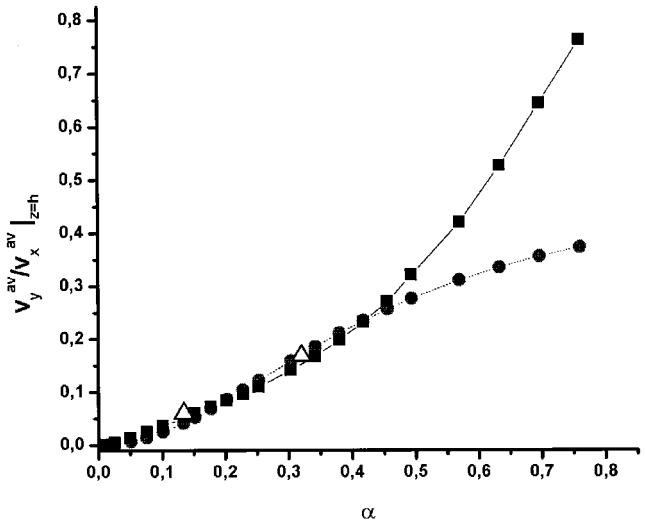

Figure 3. Boundary value of relative transverse velocity at the top of the channel.

The black squares show the CFD simulation results, the open triangles experimental values taken from Stroock et al. (2002a), and the gray circles show the results of the analytical correlation based on a simplified model (Ajdari, 2002; Stroock et al., 2002a). The lines are guides to the eye.

nents in the x-direction and y-direction were averaged over the center patch shown in Figure 1 being located at varying z-coordinates.

The ratio of average velocities v_y^{av}/v_x^{av} as a function of the vertical position in the channel (z-coordinate) is shown in Figure 2. The relative transverse velocity shows an almost linear increase inside the grooves, a steep increase above the grooves, changes sign, and flattens from about half the channel height to the top wall, where it reaches its maximum. The maximum value of 0.052 agrees quite well with the experimentally derived result of 0.06 (Stroock et al., 2002a).

Next, a series of simulations was performed varying the relative structure height α from 0.01 to 0.76. The corresponding maximum relative transverse velocities (that is, the boundary values at the top) are shown in Figure 3 with filled squares. The experimental results for $\alpha = 0.134$ and $\alpha = 0.32$ are indicated as open triangles (Stroock et al., 2002a). The gray circles in Figure 3 show the analytical results of Stroock et al. (2002a). [For their derivation see also Ajdari (2002).] First, one notices the good agreement between simulation and experiment for both values of α. Second, one finds a good agreement between the numerical results and the analytical approximation for $\alpha < 0.45$. Surprisingly, the approximation yields reasonable results up to relatively large values of α, although it is strictly valid only in the limit $\alpha \ll 1$. However, the error of the approximation increases rapidly for $\alpha > 0.45$.

In a next set of simulations the relative transverse velocities of single-sided and double-sided structured channels are compared. For this purpose additional bas-relief structures on the top wall, as indicated in the right part of Figure 1, were assumed. For the numerical implementation an unstructured grid with about $1.4 \cdot \times 10^6$ cells was used.

Figure 4 shows a typical simulation result for $h = 0.79$ mm, $\alpha = 0.134$, and $w = 0.2$ mm. As to be expected, we find a symmetric curve in case of structures on two opposite channel walls with a point of reflection at $h/2$. Both curves almost coincide except for the regions close to the top of the channel. The absolute transverse velocity, which causes the tilting of incoming fluid lamellae and thereby increases the interfacial area, is directly correlated to the mixing efficiency. Thus a considerably improved mixing performance is to be expected by the use of structures on opposite channel walls.

This is also illustrated by the series of cross sections shown in Figure 5, displaying the convective entanglement of two initially vertical liquid lamellae. The first cross section is taken right at the beginning of the structured region at $x = 0$. The

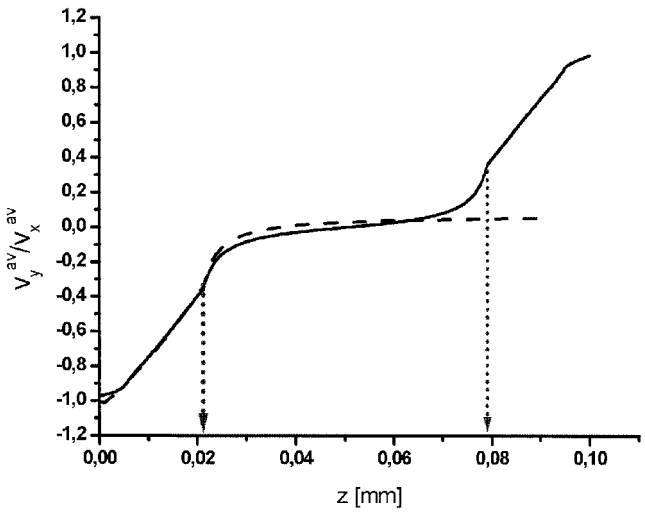

Figure 4. Comparison of relative transverse velocities in single- (dashed line) and double-sided (solid line) structured channels.

The vertical arrows mark the edges of the bas-relief structures as in Figure 2.

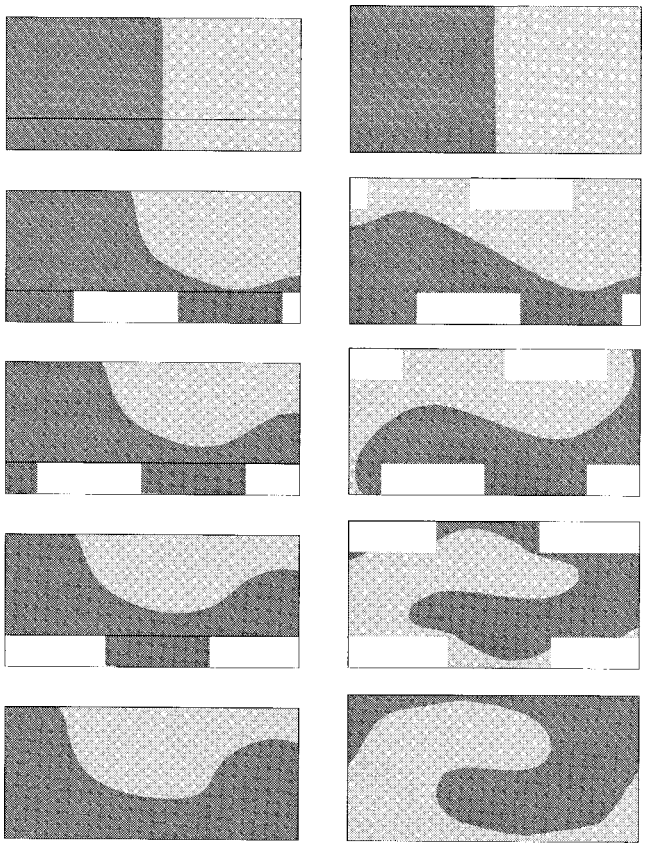

Figure 5. Comparison of wrapping of two liquid lamellae in a channel with structures on one (upper row) and on two walls (lower row).

The cross sections are taken at the beginning of the structured region ($L = 0$ mm), at $L = 0.4$ mm, $L = 0.8$ mm, $L = 1.2$ mm, and at $L = 1.6$ mm at the end of the structured region (cf. dashed lines in Figure 1).

subsequent ones are taken at positions $x = 0.4$, 0.8, 1.2, and 1.6 mm, as indicated by the dashed lines in Figure 1. By comparing the cross sections of the upper row at $x = 0.8$ and $x = 1.6$ mm with the ones of the double-sided structured channel at $x = 0.4$ and $x = 0.8$ mm, respectively, one finds a considerable increase of the lamellae entanglement and an enlarged interfacial surface area in case of bas-relief structures on two walls.

Finally, we analyzed the dependency of the relative transverse velocity on the Reynolds number. Surprisingly, we find a rather weak dependency. Although the absolute transverse velocity within the oblique ridges is considerably enhanced when increasing the Reynolds number from 1 to 1000, the relative transverse velocity above the structures is found to be only scarcely affected.

To quantify the mesh dependency of the derived results the relative transverse velocity for a single-sided structured channel (cf. Figure 2) computed on a grid with about 300,000 cells was compared to the corresponding values computed on grids with 90,000 and 440,000 cells. Using a Richardson extrapolation, that is, a linear fit of the simulation results as a function of 1/(number of grid cells), we find the result for the maximum velocity based on 300,000 cells to agree with the extrapolated value within an error of less than 1%.

Simulation of Helical Flow in Curved Channels

Subsequently, secondary flows in rectangular channels without surface corrugations are analyzed, particularly with respect to their use for induction of chaotic mixing. Because of the action of centrifugal forces a secondary flow develops in curved pipes and channels. The characteristic feature is a shift of the maximum in the velocity profile toward the outer channel wall accompanied by the occurrence of Dean vortices (Dean, 1927, 1928). The occurrence of Dean vortices in curved channels has been intensively studied in various contexts as filtration (Bubolz et al., 2002a,b), heat exchange (Cheng and Akiyama, 1970), friction (Cheng et al., 1976; Hart et al., 1988), and also mixing (Schierholz et al., 1997), to name a few.

Typical patterns in this context are two counterrotating vortices, above and below the symmetry plane of the channel, coinciding with its plane of curvature. In that symmetry plane fluid is transported in the outward direction by centrifugal forces and is transported back by recirculation along the channel walls. The dimensionless groups characterizing such types of flow are the Reynolds number

$$\mathrm{Re} = ud/\nu \tag{3}$$

where u, d, and ν denote the mean velocity, the hydraulic diameter, and the kinematic viscosity, respectively, and the Dean number

$$K = \mathrm{Re}(d/R)^{1/2} \tag{4}$$

where R is the radius of curvature. A qualitative change in the secondary flow pattern is observed for Dean numbers above a critical value K_c of about 200. For $K < K_c$, the secondary flow consists of two counterrotating vortices, whereas for $K > K_c$ two additional counterrotating vortices appear close to the center of the outer channel wall (Cheng et al., 1976). A consecutive change of the geometry parameters (hydraulic diameter or radius of curvature) or the Reynolds number, such that the Dean number changes from $K < K_c$ to $K > K_c$ and vice versa, allows switching between the two different flow patterns.

To study such secondary flows with regard to mixing applications, a CFD model was set up. The model geometry of the curved square channel used in the simulations is depicted in Figure 6. Because reflection symmetry with respect to the r–φ plane is exploited, only half the geometry was modeled and is

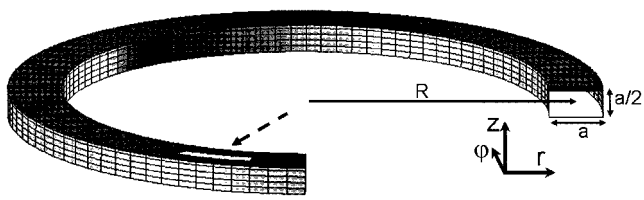

Figure 6. Model geometry of the curved square channel used in the simulations.

Because reflection symmetry with respect to the r–φ plane is exploited, only half the geometry is shown. a and R denote the channel dimension and the radius of curvature, respectively. The dashed arrow marks the patch used for averaging of the velocity components.

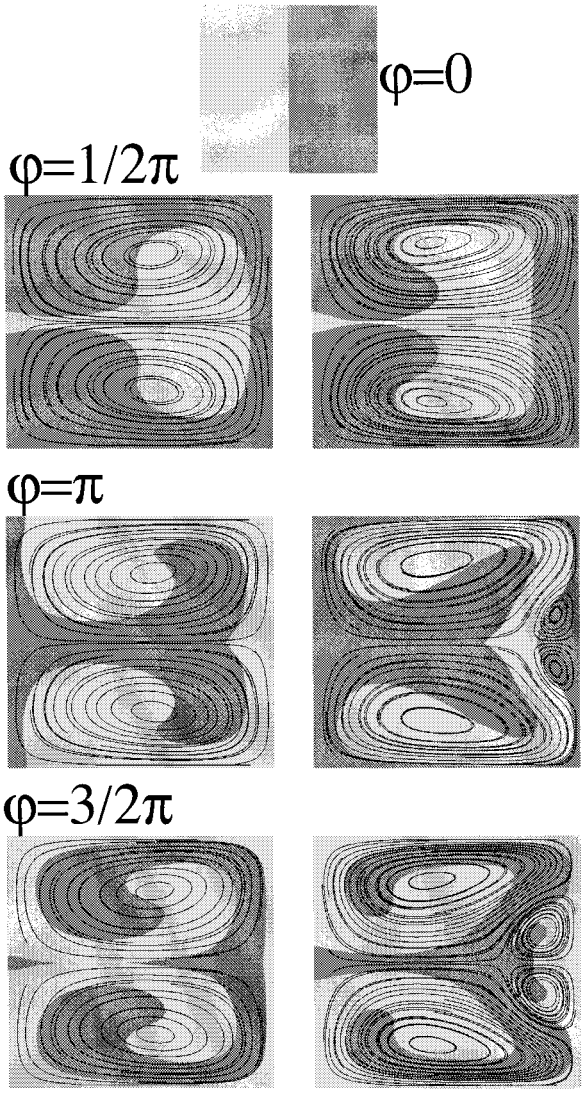

Figure 7. Cross sections at the inlet, outlet, and at two intermediate positions for two Dean numbers, $K = 150$ (left column) and $K = 300$ (right column).

The initial condition for the species concentration (encoded in gray) is shown in the leftmost figure (that is, two lamellae oriented parallel to the z-axis). Additionally, the velocity fields of the secondary flow are shown for $\varphi > 0$.

shown in the figure. A structured mesh with about 200,000 cells was used, where the height and width of the channel were resolved with 18 and 36 cells, respectively. Because of graphical reasons a considerably coarser mesh is shown in the figure. Simulations were performed for Dean numbers K ranging from 1 to 900, corresponding to Reynolds numbers between 2 and 2012 for the chosen radius $R = 5d$.

Figure 7 shows cross sections at the inlet, outlet, and at two intermediate positions for two Dean numbers, $K = 150$ (left column) and $K = 450$ (right column). As shown in the upper figure, the initial condition for the species concentration (encoded in gray) is given by two lamellae oriented parallel to the z-axis. Additionally, the velocity fields of the secondary flow are shown for $\varphi > 0$. The velocity profiles at the beginning at $\varphi = \pi/2$ are qualitatively identical, leading to similar concentration distributions. At $\varphi = \pi/2$ an additional pair of counter-rotating vortices develops close to the center of the outer (right) channel wall for $K = 450$. The occurrence of the additional vortices, developing right from the start, causes the incomplete displacement of the right (dark gray) lamella. In this case, the complete liquid volume, shaded in dark gray, is not transported to the left side of the channel, but a certain fraction remains on the right side. Finally, at $\varphi = 3/2\pi$ a steady velocity profile with four vortices is well developed.

Figure 8 shows a magnification of the secondary flow velocity profile at $\varphi = 7/5\pi$. Here, the gray scale encodes the positive part of the secondary flow vorticity, defined as

$$f(r, z) = \Theta[\vec{e}_{\perp}(\vec{\nabla} \times \vec{v}_{proj})] \tag{5}$$

where $\vec{v}_{proj}$ is the secondary flow velocity, that is, the projection of the total velocity onto the (r, z) plane; $\vec{e}_{\perp}$ denotes the unit normal; and Θ is the step function. In the above notation the vorticity of the main vortex in the upper half is less than zero; the step function Θ is introduced to allow for a vorticity analysis of the outer vortex independent of the main one.

As a measure of the total vorticity of the side vortices under consideration, the function $f(r, z)$ was integrated over the relevant part of the cross section, which is marked with the black rectangle in Figure 8. The integration area was restricted to the shown square to minimize boundary effects originating from the velocity gradient at the channel walls. The integrals as a function of Dean number are shown in Figure 9. As can be read off from the curve the additional vortices start to develop at Dean numbers around 200. The strongest increase of the vorticity is observed at Dean numbers between 300 and 400.

To our knowledge the occurrence of additional vortices in rectangular channels for high Dean numbers was first discussed by Cheng et al. (1976). Based on a two-dimensional (2-D) finite-difference approach, these authors find the same result for the critical Dean number above which additional vortices appear. However, in contradiction to the results discussed above, they claim that the additional vortices disappear above an upper critical value, which is around $K = 500$. In our simulations disappearance of vortices was not observed for

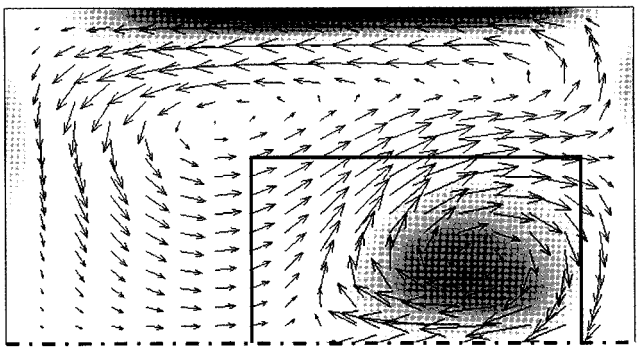

Figure 8. Magnification of the secondary flow velocity profile at $\varphi = 7/5\pi$.

The gray scale encodes the positive part of the secondary flow vorticity $f(r, z)$ defined in Eq. 5. The inner rectangle marks the area used for integration of $f(r, z)$. The dashed dotted line denotes the symmetry plane.

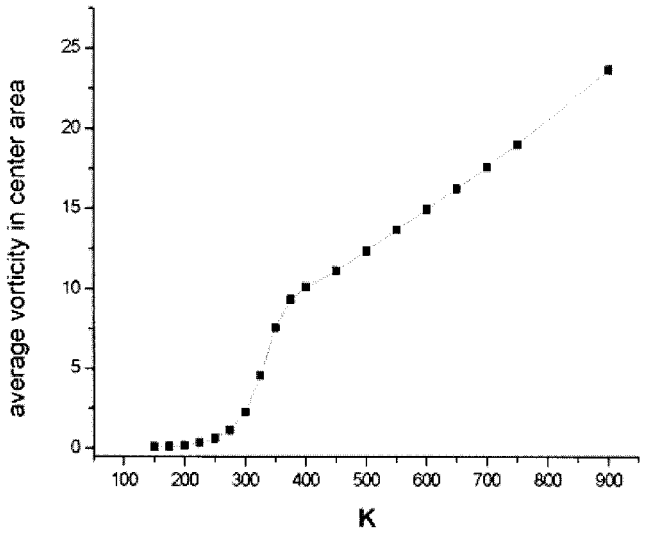

Figure 9. Total secondary vorticity [that is, integrals of $f(r, z)$], as defined in Eq. 5 over the rectangle marked in Figure 8, as a function of the Dean number.

Dean numbers between 200 and 900, which is the largest value studied.

For the velocity profiles studied we find that entrance flow effects typically dominate over a length of about πR. However, assuming the length of the entrance flow region to be $L_{in} = 0.03\mathrm{Re}\, d$ (Faber, 1995), with Reynolds number Re and hydraulic diameter d, the relative inlet length (that is, L_{in} over $2\pi R$) is given by $0.03/(2\pi)K^2/\mathrm{Re}$. Thus, generally, entrance flow effects are of particular importance in high Dean number flows.

To check for the mesh dependency of the derived results based on 200,000 cells additional simulations on grids of 400,000 and 800,000 hexahedral cells were performed. Using a Richardson extrapolation we find the result, for example, for the integral of the vorticity function (Eq. 5) for $K = 700$ to agree with the extrapolated value within an error of about 10%.

To compare the strength of the helical flow in curved channels with that in bas-relief structured microchannels as analyzed above, further simulations were performed for a square channel with a width of 0.2 mm and a radius of 1 mm. For comparison the averaged relative transverse velocity was computed as in the previous section. The patch over which averaging was performed is shown in white in Figure 6 and marked with an arrow. As above, the patch is placed in the channel center; however, here it is located close to the outlet to ensure a well-developed flow profile. The corresponding averaged relative transverse velocities are shown in Figure 10 for a series of Dean numbers. As can be read off from the figure, the curves fall into two classes with respect to their Dean number. At $K = 200$ the second pair of vortices has not yet developed, whereas at $K = 400$, 600, and 800 two pairs of vortices exist, yielding curves with an intermediate maximum of the relative transverse velocity. For Dean numbers between 400 and 800 the relative transverse velocity varies only weakly.

Furthermore, comparing the values of the relative transverse velocity with corresponding ones for bas-relief structured channels one finds them to be of similar order of magnitude. Thus, efficient micromixing can also be achieved using the very simple geometry of a curved rectangular channel.

Aref (1984) showed that efficient stirring and chaotic mixing can be achieved by an unsteady potential flow. This can, for instance, be induced by a so-called blinking vortex, that is, a vortex that discontinuously changes between two positions. In a similar sense Stroock et al. (2002b) suggested speeding up mixing by chaotic flow patterns based on alternating helical flows. The corresponding flow patterns are induced by so-called staggered-herringbone structures along one channel wall.

An analogous effect can also be accomplished with the helical flows in curved channels, without the need to introduce any additional microstructures. Again, the basic idea is to switch between different flow patterns to induce chaotic advection, as proposed by Aref (1984).

There are at least two different ways of achieving this task. First, a repeated change of the geometrical parameters a and R allows altering the Dean number and repeatedly switching between the flow regimes above and below the critical Dean number of about 200 (that is, to switch between flow patterns with two and four counterrotating vortices). Second, as can be seen from the velocity profiles shown in Figure 7, for $K = 300$ the additional vortices exhibit after a characteristic length of about πR. Hence, alternating flows can also be achieved by repetitive induction of entrance flow effects. In a corresponding geometry the flow, after having assumed its fully developed profile, would be directed out of a channel section into a new curved channel, where again the pattern with four counterrotating vertices would take some time to develop. Alternatively, switching between different flow patterns and entrance flow effects can also be induced by simply changing the sign of curvature. The corresponding geometry of a meandering channel is shown in Figure 11. In contrast to the case of two vortices, where an alteration of the sign of the channel curvature basically reverses the secondary flow, a chaotic flow is induced by periodic changes

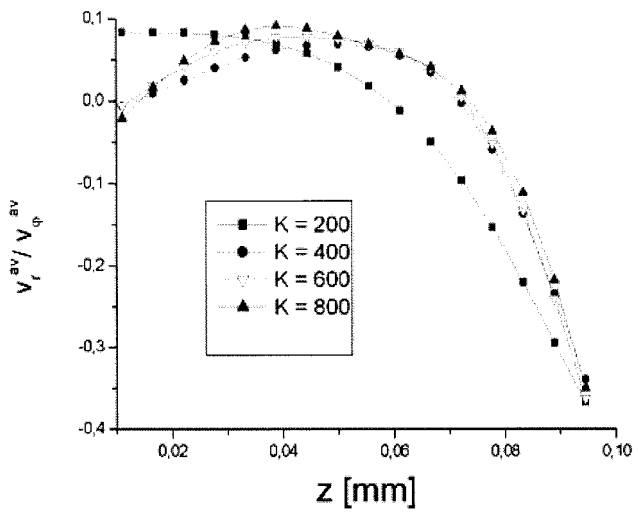

Figure 10. Relative transverse velocities averaged over the patch shown in Figure 6 for Dean numbers between 200 and 800.

$z = 0$ and $z = h/2$ corresponds to averaging over the center patch in the symmetry plane and at the top wall, respectively.

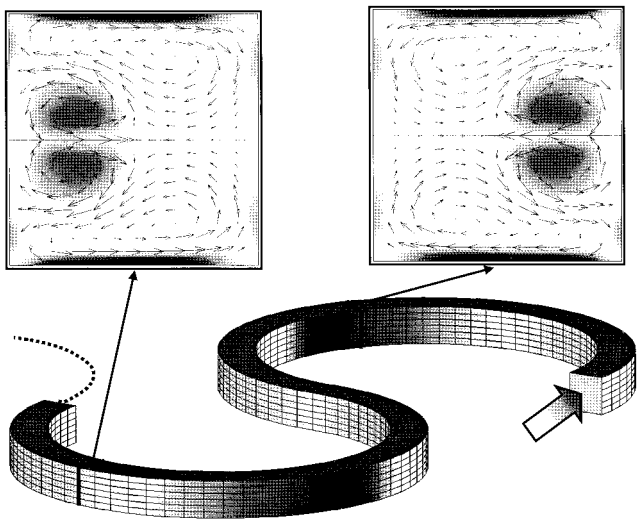

Figure 11. Bottom: sketch of a meandering channel buildup from circular segments as shown in Figure 6.

The arrow indicates the flow direction, the dashed line the continuation of the geometry. Top: Cross-sectional view of secondary flows taken in flow direction.

of the curvature for large Dean numbers (that is, for secondary flow pattern with four vortices). This is illustrated by the secondary flows shown in a cross-sectional view for different segments of the meandering channel.

Either of these approaches will lead to a chaotic flow pattern similar to the one described in Stroock et al. (2002b), having been achieved with alternating bas-relief structures. A thorough analysis of the induced chaotic flows by means of Poincaré maps derived from streamline-tracking is subject of a forthcoming analysis.

Summary and Conclusions

In this article helical flows in microchannels were studied using CFD methods. Special attention was paid to the aspect of micromixing, which is an important issue for many applications in the field of Lab-on-a-Chip and μ-TAS systems. The first part of the article was focused on helical flows in bas-relief structured microchannels, a topic previously investigated by Stroock et al. (2002a,b) and others (Johnson et al., 2001, 2002; Kim et al., 2002). The CFD results were found to be in good agreement with these experimental results. It was shown that the analytical model used by Stroock et al. (2002b) yields good results up to surprisingly large values of the depth of the groovelike microstructures ($\alpha = 0.45$). However, in general, CFD models are necessary to reliably predict the growth of interfacial area per unit length of the mixing channel for initially adjacent liquid lamellae. A large potential for speeding up mixing is expected by the exploitation of chaotic flow patterns that can be induced by periodically changing the geometry of the mixing channel. In this context it was shown that bas-relief structures on two opposite walls lead to a significant increase of the relative transverse velocity compared to channels with structures on only one wall. The corresponding cross-sectional views of the lamellae structure show an enlarged interfacial surface area.

The main objective of the second part of the article was to show that similar chaotic flow patterns can also be induced with a simpler geometry relying on curved channels. Here, a concept was proposed relying on different types of Dean vortices occurring in curved channels. Accordingly, chaotic flows are generated by periodic "switching" between two different flow patterns with two and four Dean vortices, respectively. An alternating sequence of such flow patterns can be induced, for example, by repetitive changes of the Dean number of the flow or by repetitively forcing the flow into a channel entrance. In accordance with Cheng et al. (1976), the additional Dean vortices were found to appear at Dean numbers in the range of 200. However, we have found the four-vortex pattern to be stable up to large Dean numbers.

Similarly to the previous studies for the microchannels with bas-relief structured the relative transverse velocity was computed to assess the potential of curved channels for micromixing. It was found that for the two different helical flow patterns transverse flow velocities of similar order of magnitude can be obtained. Correspondingly, cross-sectional views of the flow show a considerable entanglement of liquid lamellae.

Thus, curved channels, especially when arranged in such a way that chaotic flow patterns are induced, lend themselves for speeding up mixing in microfluidic systems. Such channels are in general easier to fabricate than bas-relief structured channels because they do not require multistep structures. Additional applications may be found in systems where an increased heat or mass transfer or a reduction of hydrodynamic dispersion is required.

Literature Cited

Ajdari, A., "Transverse Electrokinetic and Microfluidic Effects in Micro-Patterned Channels: Lubrication Analysis for Slab Geometries," *Phys. Rev. E*, **65**, 016301 (2002).

Aref, H., "Stirring by Chaotic Advection," *J. Fluid. Mech.*, **143**, 1 (1984).

Bubolz, M., G. Langer, P. Walzel, and U. Werner, "Simulation der Deckschichtbildung bei der Querstromfiltration mit Dean-Wirbeln," *Chem.-Ing.-Tech.*, **11**, 1601 (2002).

Bubolz, M., M. Wille, G. Langer, and U. Werner, "The Use of Dean Vortices for Crossflow Microfiltration: Basic Principles and Further Investigation," *Sep. Pur. Technol.*, **26**, 81 (2002).

CFX-4.2 Solver Manual, AEA Technology, Oxfordshire, UK (1997).

Cheng, K. C., and M. Akiyama, "Laminar Forced Convection Heat Transfer in Curved Rectangular Channels," *Int. J. Heat Mass Transfer*, **13**, 471 (1970).

Cheng, K. C., R.-C. Lin, and J.-W. Ou, "Fully Developed Laminar Flow in Curved Rectangular Channels," *J. Fluids Eng.*, **March**, 41 (1976).

Dean, W. R., "Note on the Motion of a Curved Pipe," *Philos. Mag.*, **4**, 208 (1927).

Dean, W. R., "The Stream-Line Motion of Fluid in a Curved Pipe," *Philos. Mag.*, **5**, 673 (1928).

Ehrfeld, W., K. Golbig, V. Hessel, H. Löwe, and T. Richter, "Characterization of Mixing in Micromixers by a Test Reaction: Single Mixing Units and Mixer Arrays," *Ind. Eng. Chem. Res.*, **38**, 1075 (1999).

Ehrfeld, W., V. Hessel, and H. Löwe, *Microreactors*, Wiley-VCH, Weinheim, Germany (2000).

Faber, T. E. *Fluid Dynamics for Physicists*, Cambridge Univ. Press, Cambridge, UK (1995).

Fletcher, C. A. J. *Computational Techniques for Fluid Dynamics 1*, 2nd ed., Springer-Verlag, Berlin (1997).

Hart, J., K. Ellenberger, and P. J. Hamersma, "Single- and Two-Phase Flow Through Helically Coiled Tubes," *Chem. Eng. Sci.*, **43**(4), 775 (1988).

Johnson, T. J., and L. E. Locascio, "Characterization and Optimization of Slanted Well Designs for Microfluidic Mixing under Electroosmotic Flow," *Lab Chip*, **2**, 135 (2002).

Johnson, T. J., D. Ross, and L. E. Locascio, "Rapid Microfluidic Mixing," *Anal. Chem*., **74**, 45 (2001).
Kim, D. S., S. W. Lee, T. H. Kwon, and S. S. Lee, "Barrier Embedded Chaotic Micromixer," *Micro Total Anal. Syst.*, **2**, 757 (2002).
Noll, B., *Numerische Strömungsmechanik*, Springer-Verlag, Berlin (1993).
Sawyers, D. R., M. Sen, and H.-C. Chang, "Effect of Chaotic Interfacial Stretching on Bimolecular Chemical Reaction in Helical-Coil Reactors," *Chem. Eng. J*., **64**, 129 (1996).
Schierholz, W., G. Lauschke, and S. Ott, Ger. Pat. DE 19731891 (1997).
Schwesinger, N., T. Frank, and H. Wurmus, "A Modular Microfluid System with an Integrated Micromixer," *J. Micromech. Microeng*., **6**, 99 (1996).
Stroock, A. D., S. K. W. Dertinger, A. Ajdari, I. Mezić, H. A. Stone, and G. M. Whitesides, "Chaotic Mixer for Microchannels," *Science*, **295**, 647 (2002).
Stroock, A. D., S. K. W. Dertinger, G. M. Whitesides, and A. Ajdari, *Anal. Chem.*, **74**, 5306 (2002).
Yang, Z., S. Matsumoto, H. Goto, M. Mastumoto, and R. Maeda, "Ultrasonic Micromixer for Microfluidic Systems," *Sens. Actuators A*, **93**, 266 (2001).

Manuscript received Mar. 27, 2003, and revision received Aug. 18, 2003.